


# Effects of TPU on the mechanical properties, fracture toughness, morphology, and thermal analysis of 3D-printed ABS-TPU blends by FDM

Kianoosh Soltanmohammadi<sup>1</sup> | Davood Rahmatabadi<sup>1</sup>  |  
 Mohammad Aberoumand<sup>1</sup> | Elyas Soleyman<sup>1</sup> | Ismaeil Ghasemi<sup>2</sup> |  
 Majid Baniassadi<sup>1</sup> | Karen Abrinia<sup>1</sup> | Mahdi Bodaghi<sup>3</sup> | Mostafa Baghani<sup>1</sup>

<sup>1</sup>School of Mechanical Engineering, College of Engineering, University of Tehran, Tehran, Iran

<sup>2</sup>Faculty of Processing, Iran Polymer and Petrochemical Institute, Tehran, Iran

<sup>3</sup>Department of Engineering, School of Science and Technology, Nottingham Trent University, Nottingham, UK

## Correspondence

Mahdi Bodaghi, Department of Engineering, School of Science and Technology, Nottingham Trent University, Nottingham NG11 8NS, UK.  
 Email: [mahdi.bodaghi@ntu.ac.uk](mailto:mahdi.bodaghi@ntu.ac.uk)

Mostafa Baghani, School of Mechanical Engineering, College of Engineering, University of Tehran, Tehran, Iran.  
 Email: [baghani@ut.ac.ir](mailto:baghani@ut.ac.ir)

## Abstract

In this paper, blends of ABS-TPU with two different weight percentages of TPU were prepared using fused deposition modeling technology. The effect of adding TPU on the fracture toughness of ABS and mechanical properties was comprehensively studied. Tensile, compression, fracture toughness, and shear tests were conducted on the 3D-printed samples. Thermal and microstructural analyses were performed using dynamic mechanical thermal analysis (DMTA), and scanning electron microscope (SEM). The DMTA results showed that adding TPU decreased the storage modulus and the glass transition temperature of ABS, as well as its peak intensity. The mechanical test results showed that adding TPU decreased the strength but increased the formability and elongation of the samples. Fracture tests showed that the addition of TPU decreased the maximum force needed for a crack to initiate. The force required for crack initiation decreased from 568.4 N for neat ABS to 335.3 N for ABS80 and 123.2 N for ABS60. The ABS60 blend exhibited the highest strength against crack growth, indicating that TPU can change the behavior of ABS from brittle to ductile. Shear test results and SEM images also showed good adhesion strength between the printed samples for all three specimens, indicating their good printability. Adding TPU resulted in a reduction in the size and number of voids and holes between the printed layers.

## Highlights

- Melt mixing, filament preparation, and 3D printing of ABS-TPU blends.
- Investigation of mechanical properties, microstructure, and fracture toughness.
- Improved resistance to crack growth and elongation by adding TPU to ABS.
- Improving printability and reducing microholes in blends compared with ABS.
- Achieving a wide range of mechanical properties for various applications.

This is an open access article under the terms of the [Creative Commons Attribution](https://creativecommons.org/licenses/by/4.0/) License, which permits use, distribution and reproduction in any medium, provided the original work is properly cited.

© 2024 The Authors. Journal of Vinyl & Additive Technology published by Wiley Periodicals LLC on behalf of Society of Plastics Engineers.

**KEYWORDS**

ABS-TPU blends, fracture toughness, fused deposition modeling, mechanical properties, toughening

## 1 | INTRODUCTION

Additive manufacturing (AM) is a notable method that differs from traditional manufacturing. It is utilized in academia and various industries, such as automotive, soft robotics, fashion, healthcare, and biomedical applications.<sup>1–3</sup> AM is employed to create prototypes or final parts with either simple or complex geometries. This manufacturing process entails depositing layers of material and constructing solid parts with precise geometric shapes.<sup>4,5</sup> The process begins with a computer-aided design model, which is then sliced into layers of equal thickness to ensure high quality and resolution.<sup>6</sup>

Among the different AM technologies used for various types of materials, such as metals, ceramics, and polymers, fused deposition modeling (FDM) stands out as one of the most efficient and cost-effective techniques for producing thermoplastic parts.<sup>7–9</sup> FDM involves extruding semiliquid thermoplastic material, which aligns with the core concept of AM.<sup>10</sup> The raw materials used in this method are filaments, which are typically heated to a molten state and then extruded through the nozzle of the 3D printer.<sup>11,12</sup> However, as FDM has evolved, there has been a demand for materials tailored to specialized applications in different fields. These materials require appropriate mechanical, biological, and physical characteristics. Therefore, over the past decade, numerous experimental and numerical studies have focused on improving the FDM technique in various aspects. These include enhancing the mechanical properties of the materials used during FDM. Different methods can be used to enhance the properties of the materials used in FDM. These methods include, as mentioned earlier, embedding reinforcements (short and continuous fibers) and nanoparticles as fillers into the polymer/thermoplastic or polymer blending and toughening.<sup>13,14</sup> Polymer toughening is particularly important in eliminating the limitations of the polymers and thermoplastics used in FDM.<sup>12</sup>

Acrylonitrile butadiene styrene (ABS) is a commonly used thermoplastic polymer in FDM when it is extruded into a filament. ABS is cheap, strong, and stable and it can undergo various postprocessing methods such as sanding, painting, gluing, filling, and chemical smoothing. However, when ABS is 3D-printed using the FDM process, its low toughness and high tendency to shrinkage become issues. Therefore, due to the recent interest

in fabricating functional parts like actuators or shock absorbers from thermoplastics, especially ABS and its limitations when 3D-printed using FDM, researchers have employed different methods to achieve high mechanical properties of ABS-based 3D-printed components.<sup>15,16</sup> In addition to incorporating fillers such as graphite, short and continuous carbon fibers, metals, and lignin, several groups have created printable composites based on ABS by blending ABS with other polymers. Thermoplastic elastomers (TPEs), including vulcanized rubber (TPV), styrene (TPS), and polyurethane (TPU), are potential additives for ABS due to their excellent adhesive properties. Blending and toughening ABS is considered one of the most efficient and cost-effective ways to enhance its properties. Some studies have focused on toughening ABS using various elastomers and plasticizers.<sup>16–20</sup> In addition to enhancing the mechanical properties of ABS, another benefit of ABS toughening is a decrease in the glass transition temperature when it is blended with compatible materials.<sup>16,19</sup> de León et al.<sup>20</sup> conducted a study in which they prepared a series of ABS-TPU blends with varying weight percentages (10, 20, and 30 wt%) for use in 3D printing via FDM. ABS was used as the main material, whereas TPU was added as an additive. The researchers successfully determined the optimal printing parameters for the ABS-TPU blends and investigated their printability, as well as their mechanical and adhesive properties in different directions. They also examined the compatibility between ABS and TPU. The researchers discovered that the addition of TPU increased elongation. They also observed that the adhesion between layers improved when up to 20 wt% TPU was added, and there was no reduction in yield strength. However, when the TPU content was increased to 30 wt%, the yield strength of the blends became more similar to that of TPU (20 MPa) rather than ABS (29.3 MPa), while the bonding between layers was enhanced. Thavornnyutikarn et al.<sup>21</sup> mixed ABS-TPU blends with three different percentages and after preparing the filament and extracting the optimal printing parameters, they found that with the increase of TPU, the amount of warpage of the ABS-TPU decreases compared with pure ABS. Also, TPU increased the plasticity and softening of the fracture cross-section, and the blend containing the most TPU had better print quality and surface roughness.

Weng et al.<sup>22</sup> reported a 43% increase in the tensile strength of ABS 3D-printed components by adding just

5 wt% of organically modified montmorillonite (OMMT). They also observed significant improvements in the tensile and flexural strength, as well as the dynamic mechanical storage modulus. In addition, the authors noted a decrease in the linear thermal expansion ratio and weight loss, as measured by thermogravimetric analysis (TGA). Based on these findings, they suggested that this novel ABS-OMMT nanocomposite exhibits superior mechanical and thermal properties, making it a promising material for use in the FDM process. Zhu et al.<sup>23</sup> assessed the effects of adding styrene-acrylonitrile (SAN) on the mechanical properties, melt flow index (MFI), and glass transition temperature ( $T_g$ ) of ABS-SAN blends used in the FDM process. They observed an increase in the tensile strength and modulus of the blends but a decrease in MFI and elongation at break. No significant changes were observed in the glass transition temperature.

Siqueiros et al.<sup>16</sup> developed a new printable material by melt blending of ABS with TPE styrene ethylene butylene grafted with maleic anhydride (SEBS-g-MA) at various concentrations. The elongation at break values improved from 8.5% for neat ABS to approximately 50% for ABS/SEBS-g-MA 50/50 composition. In another study, Akato et al.<sup>24</sup> investigated the dynamic mechanical properties of ABS blended with biomass-derived lignin. They blended ABS with lignin of varying contents and prepared blends by adding 10 wt% Poly(ethylene oxide) (PEO) (relative to the amount of lignin). The researchers reported compatibility between ABS and lignin, with no loss in mechanical properties. Initially, the addition of lignin improved the tensile strength, but further addition led to a decrease. However, the addition of PEO enhanced the interfacial adhesion.

In the present research, we prepared a series of ABS-TPU blends with 20% and 40% TPU by weight and 3D printed them using the FDM machine. The objective of this is to investigate the mechanical properties of ABS when reinforced with TPU and compare them with those of pure ABS and TPU. Furthermore, we conducted a shear test to assess the adhesion between TPU and both the toughened and pure ABS materials.

## 2 | EXPERIMENTAL PROCEDURES

### 2.1 | Materials and filament preparation

In the first step, ABS and TPU granules with a grade of 365A were purchased and prepared from Baspar Chemi Sepidan Co. (Tehran, Iran) and Xiamen Keyuan Plastic Co., Ltd (Fujian, China), respectively. After being dried at a temperature of 80°C for 3 h, ABS and TPU were blended, and ABS-TPU blends were fabricated with 20%

and 40% of TPU (ABS80 and ABS60) using a Coperion twin-screw extruder with an  $L/D$  of 40 and a screw diameter of 25 mm. The process temperature ranged from 200 to 220°C, and the screw speed was fixed at 70 rpm.

In the next step, filaments with a diameter of 1.75 mm were prepared from neat ABS, TPU, ABS80, and ABS60 blend palettes using a hand-made single-screw extruder with an  $L/D$  of 15 and a screw diameter of 15 mm. The screw speed was set at 30 rpm, and the process temperature was 230°C.

### 2.2 | Printing procedure

For printing the prepared ABS-TPU filaments, a desktop FDM machine with a 0.8-mm diameter nozzle was used. The fill density for all samples was set at 100%, and the printing raster angle was fixed at 0°. Each printed layer had a thickness of 200  $\mu\text{m}$ . The bed temperature of 65°C was chosen based on experiments conducted by Yin et al.<sup>25</sup> and de León et al.<sup>20</sup> The printing temperatures for neat ABS, ABS blends, and TPU were set at 240, 240, and 230°C, respectively. The printing speed for neat ABS, ABS80, and ABS60 samples was 50 mm/s, whereas the speed for TPU was fixed at 15 mm/s.

### 2.3 | Materials characterizations

In this paper, flexural, uniaxial tensile, compression, and fracture toughness tests were conducted at ambient temperature to evaluate the effect of polyester-based TPU on the mechanical properties of toughened ABS-based blends. Shear tests were also conducted to assess the bonding strength of TPU with the blends or the neat ABS, and microscopic images were taken using scanning electron microscopy (SEM). All samples were printed and evaluated to ensure the accuracy of the results. Additionally, dynamic mechanical thermal analysis (DMTA) tests were performed on the blends and the neat ABS.

#### 2.3.1 | Dynamic mechanical thermal analysis

To determine the storage modulus and the glass-rubbery transition phase and temperature for all 3D-printed neat ABS and ABS (20 and 40 wt%) TPU filaments, a DMTA test was performed using a dynamic mechanical thermal analyzer (Mettler Toledo, Switzerland). The test was conducted at a temperature range of -100 to 140°C with a heating rate of 5°C/min. The test specimens were prepared in the shape of a cantilever beam with dimensions of

40 × 10 × 1 mm, following ASTM D4065-01 guidelines. The frequency of the test was set to a constant 1 Hz.

### 2.3.2 | Uniaxial tensile test

The uniaxial tensile test was conducted on 3D-printed samples with the standard geometry of ASTM-D638-Type V for neat ABS, TPU, and ABS-TPU blends. This was done using a customized servo-mechanical universal test machine (Khallagh Sanat Atieh Peyman Company, Iran). The specimens were subjected to deformation until they reached the breaking point, with a strain rate of 3 mm/min. It is important to note that the loading direction was parallel to the raster direction.

### 2.3.3 | Uniaxial compression test

The neat ABS, TPU, ABS80, and ABS60 3D-printed samples, with dimensions of 10 × 10 × 10 mm, were subjected to compressive loading using a universal testing machine (STM-50, Santam, Iran) with a capacity of 50 kN. The compression test was conducted according to the ISO604:2002 standard, which was previously used by Ratiu et al.<sup>26</sup> to study the compressive behavior of Polylactic acid (PLA), carbon fiber PLA, and PETG 3D-printed parts. The loading was applied vertically to the direction of the raster, and the maximum strain and strain rate applied to the specimens were 80% (8 mm) and 3 mm/min, respectively.

### 2.3.4 | Flexural test

The samples for the flexural test were printed in a geometry of 50 × 10 × 4 mm. A customized servo-mechanical universal test machine (Khallagh Sanat Atieh Peyman Company, Iran) was used. It was equipped with a three-point bending fixture, which had cylindrical supports with a diameter of 5 mm and a distance of 30 mm. The specimens were loaded at a strain rate of 3 mm/min until they reached the breaking point.

### 2.3.5 | Fracture toughness test

The single-edge notched bending (SENB) samples were 3D-printed to evaluate the fracture toughness behavior of neat ABS, TPU, ABS-TPU20, and ABS-TPU40. The 3D-printed SENB samples were prepared according to the ASTM D5045 standard, and fracture tests were conducted under three-point bending with a displacement rate of

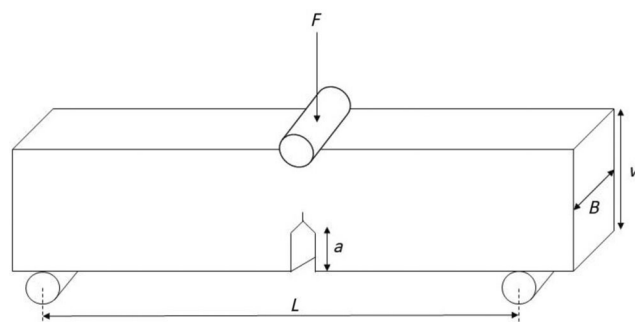


**FIGURE 1** Schematic of single-edge notched bending sample for fracture test.

1 mm/min at room temperature.<sup>28–30</sup> The SENB samples had a length of 60 mm, a width of 12 mm, a thickness of 6 mm, and an initial crack length of 5 mm. Figure 1 illustrates the geometry, dimensions, and parameters of a SENB sample.

### 2.3.6 | Shear test

For the shear test, a universal test machine (Khallagh Sanat Atieh Peyman Company, Iran) equipped with a sliding shear fixture was used. The first piece has a 5 mm depth groove, whereas the second has a hole. When these two pieces are slid against each other, neat shear force is applied to the samples. The shear test specimens were prepared to match the geometry of the fixture. The samples are in the shape of two cubes, measuring 10 × 10 × 5 mm and 8 × 8 × 5 mm. Three reference samples were printed using neat ABS, ABS80, and ABS60.

### 2.3.7 | Scanning electron microscopy

To evaluate the bond or adhesion quality between the printed layers of the materials, a SEM was used. Images were taken from the cross section of the 3D-printed samples. To prepare the samples, they were frozen and then broken down in liquid nitrogen. Afterwards, they were coated with gold before imaging. The imaging process was carried out using the Philips XL30 SEM from the Netherlands, specifically in secondary electron imaging mode.

## 3 | RESULTS AND DISCUSSION

### 3.1 | Thermal analysis

In Figure 2, the storage modulus and  $\tan \delta$  of the polyester-based TPU are depicted. According to this

**FIGURE 2** Dynamic mechanical thermal analysis curves of polyester-based TPU.

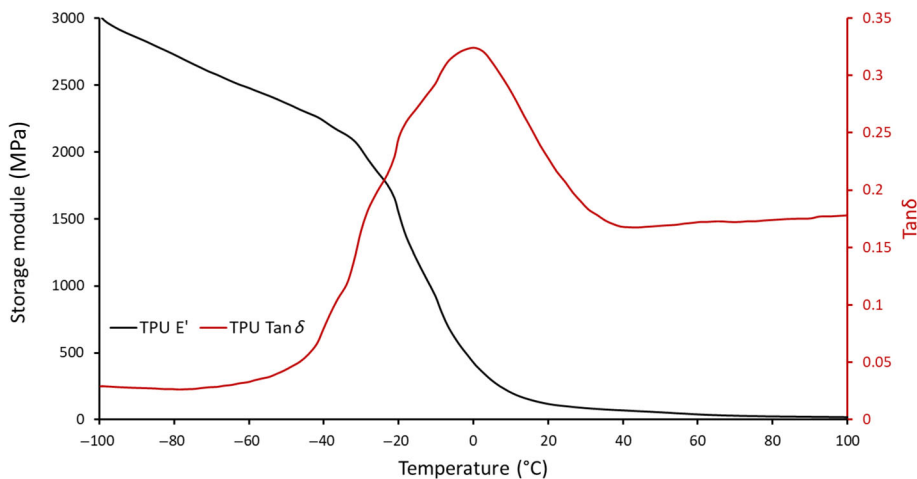
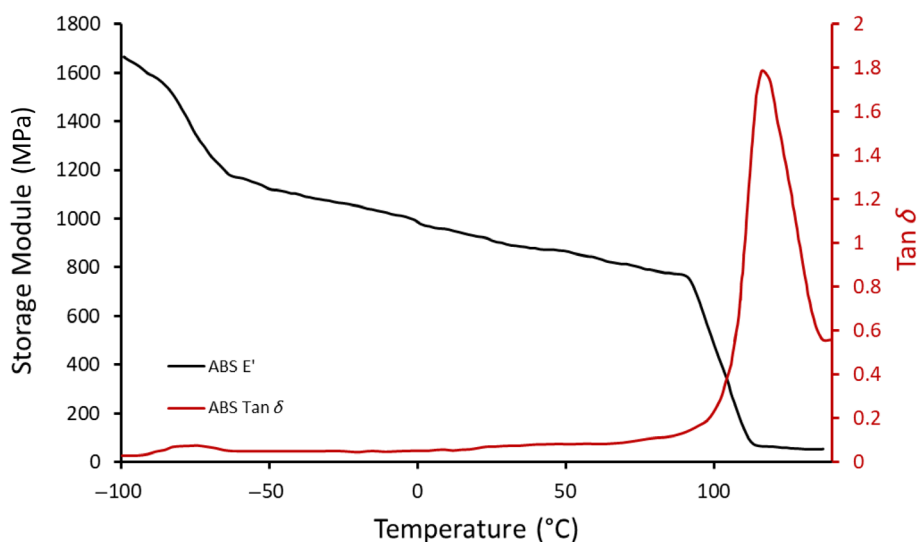


**FIGURE 3** Dynamic mechanical thermal analysis curve of the neat ABS.



figure, the  $\tan \delta$  curve remains stable between  $-100$  and  $-40^\circ\text{C}$ . However, it starts to increase around  $-40^\circ\text{C}$ , marking the beginning of the glass–rubber transition (glass–liquid transition). After reaching a peak and then experiencing a drop, the curve enters a period of stability at  $25^\circ\text{C}$ , indicating the end of the glass–rubber transition over a wide range of temperatures. The  $\tan \delta$  curve reaches its peak at approximately  $-1^\circ\text{C}$ , which serves as an indicator of the glass transition temperature of TPU. The intensity of the  $\tan \delta$  peak for TPU is about 0.325. Furthermore, the TPU's storage modulus decreases from 3000 MPa at  $-100^\circ\text{C}$  to about 80 MPa at room temperature. The curve continues to decrease until it drops to 19 MPa at  $100^\circ\text{C}$ .<sup>31</sup>

As shown in Figure 3, the glass-to-rubber transition of neat ABS begins at  $90^\circ\text{C}$  and ends at  $135^\circ\text{C}$ . There is also a peak for  $\tan \delta$  at  $118^\circ\text{C}$  ( $T_g$ ), indicating the glass transition temperature with a peak intensity of 1.8. On the other hand, the storage modulus of this material is approximately 1700 MPa at  $-100^\circ\text{C}$  and 995 MPa at  $0^\circ\text{C}$ .

It then slightly decreases to 780 MPa at  $85^\circ\text{C}$  and 900 MPa at room temperature. However, it drops sharply to 55 MPa at  $100^\circ\text{C}$ . Additionally, a  $\beta$  transition occurs for ABS in the temperature range from  $-85$  to  $-62^\circ\text{C}$ .<sup>31</sup>

In Figure 4, the DMTA curves of the ABS80 and ABS60 blends are included. de León et al.<sup>20</sup> conducted a comprehensive investigation and described the perfect compatibility between ABS and TPU. This phenomenon can be observed in the DMTA results (Figure 4), as both the storage modulus and  $\tan \delta$  curves of ABS80 and ABS60 blends in this examination are approximately similar. First, the presence of TPU in the blends lowers the glass transition temperature of ABS from  $118$  to  $114^\circ\text{C}$  and  $106^\circ\text{C}$  for ABS80 and ABS60 blends, respectively. Adding TPU also decreased  $\tan \delta$  peak from 1.8 for ABS, to 1.2 for ABS80 and 0.6 for ABS60. Furthermore, due to the compatibility of these two materials, the storage modulus of the blends decreases continuously in the examined temperature range. The initial storage modulus for ABS80 and ABS60 was approximately 1500 and



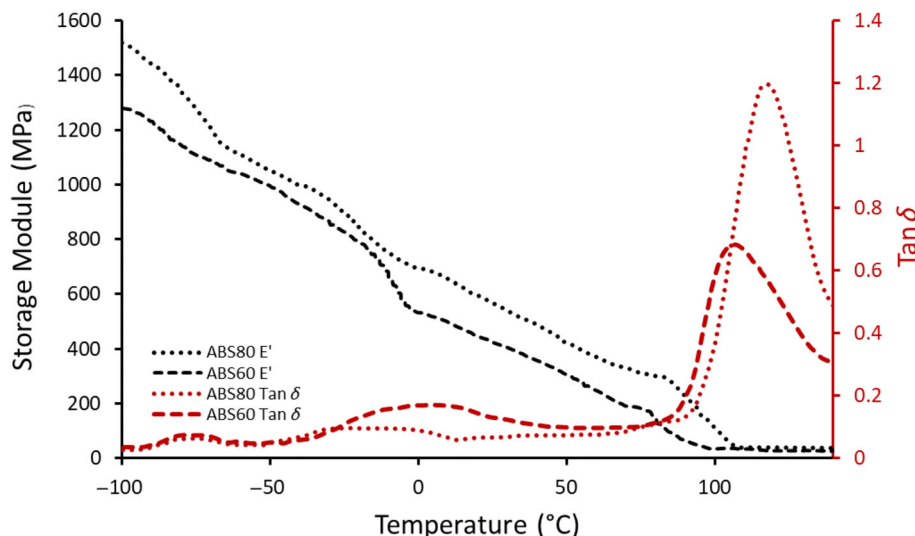


FIGURE 4 Dynamic mechanical thermal analysis curves of the ABS80% and ABS60% blends.

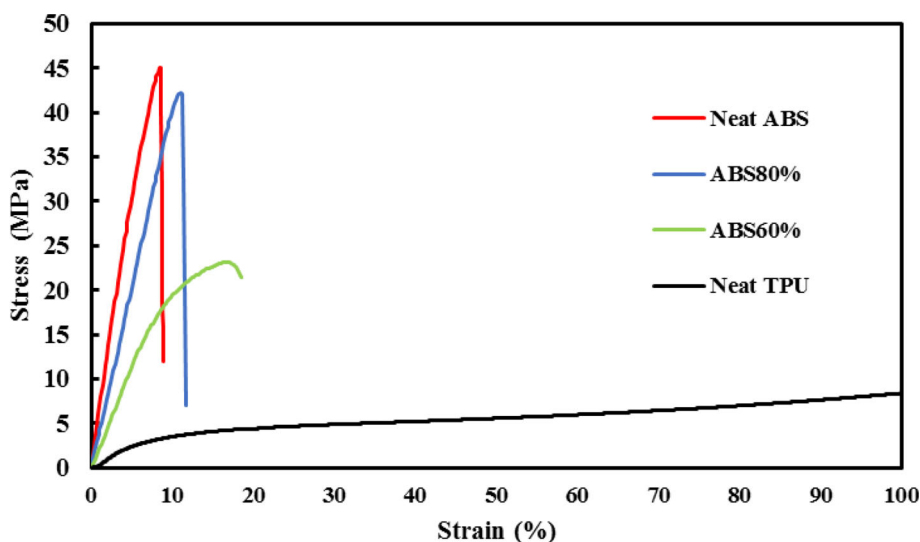


FIGURE 5 Uniaxial tensile test plots of the neat ABS, ABS80%, ABS60% and neat TPU.

1300 MPa, respectively, which is lower than that of neat ABS at 1700 MPa. The storage modulus of ABS, which is 900 MPa at room temperature dropped to approximately 600 and 400 MPa for ABS80 and ABS60, respectively.

The presence of TPU also reduces the effects of ABS's  $\beta$  transition in both blends, as seen in the DMTA curves. Other indicators of TPU's presence are the significant decline in storage modulus throughout the temperature range and substantial drops in these modulus values around 0 °C in the DMTA curves.

## 3.2 | Mechanical properties

### 3.2.1 | Uniaxial tensile and compression tests

Figure 5 illustrates the results of uniaxial tensile tests for neat ABS, TPU, ABS80, and ABS60 blends. The tensile

plots show that neat ABS has the highest elastic modulus and ultimate tensile stress (UTS), but the lowest elongation at break. TPU is also placed exactly on the opposite side of ABS. TPU has the lowest elastic modulus, tensile strength, but it has great elongation and reaches more than 300%. Based on the results, shown in Figure 5, the addition of TPU reduces the elastic modulus and UTS of the ABS-based blends, while increasing their elongation and maximum strain. The UTS and maximum strain before the breaking point are 45, 42.2, 23.2, 16.77, and 9%, 11%, 17%, 223% for neat ABS, ABS80, ABS60, and TPU respectively. Compounding the first 20 wt% of TPU with neat ABS results in a slight 6.2% drop in UTS. However, adding the second 20 wt% of TPU decreases UTS by about 45% from ABS80 and 48% from neat ABS. Blending the first and second 20 wt% of TPU increases the maximum strain by approximately 22% and 89%, respectively. Both the decrease and increase in UTS and maximum strain are nonlinear with respect to the TPU

**FIGURE 6** Uniaxial compression test plots of the neat ABS, ABS80%, ABS60%, and neat TPU.

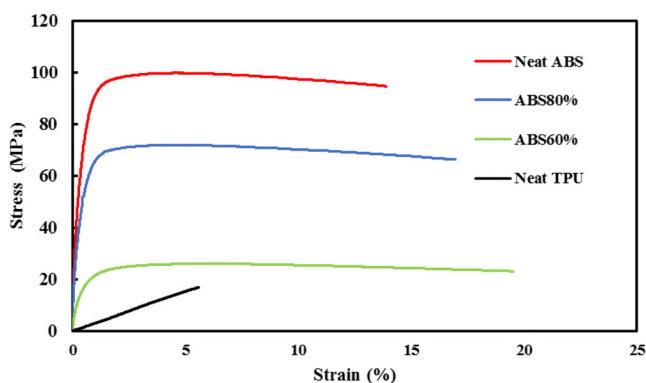
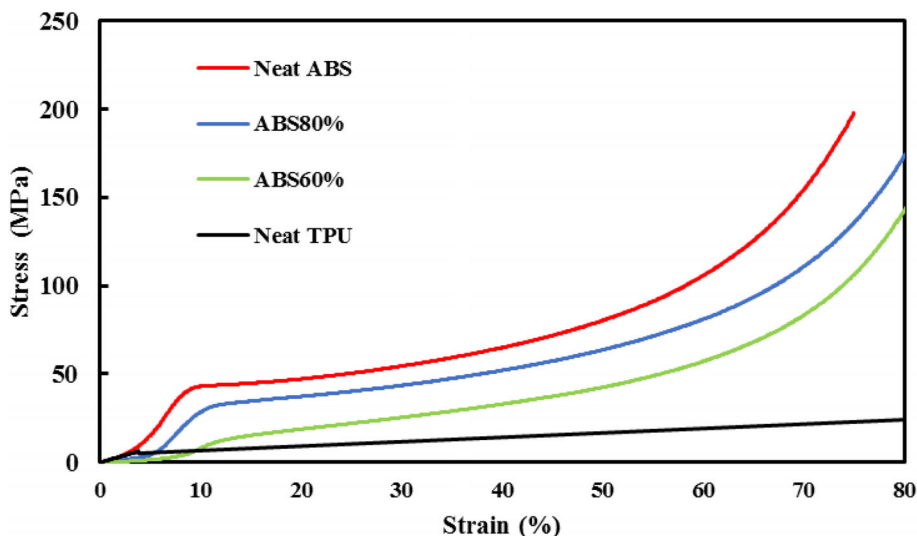


**FIGURE 7** Three point bending test plots of the neat ABS, ABS80%, ABS60%, and neat TPU.

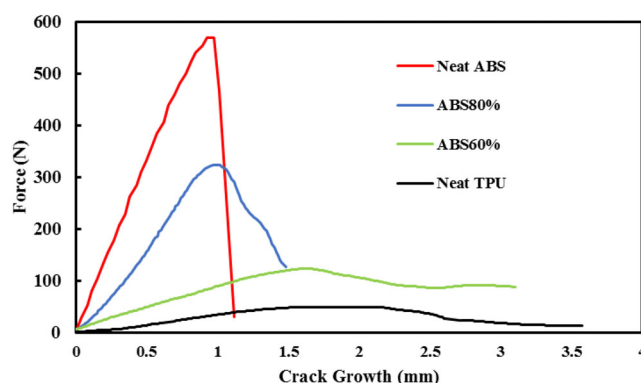


**FIGURE 8** Force-crack growth diagrams for single-edge notched bending samples of the neat ABS, ABS80%, ABS60% and neat TPU.

portion, and there is a significant jump with the addition of the second 20 wt% of TPU.

According to the uniaxial compression test plots shown in Figure 6, the samples were able to withstand a high strain of 75% due to the compression stress causing crack closure.<sup>27</sup> The yield strength of the neat ABS, ABS80, ABS60, and TPU is 40.4, 29.5, 11.3, and 6.1 MPa respectively. A significant 27% drop in yield strength is observed by adding the first 20 wt% of TPU. Blending the next 20 wt% of TPU results in substantial decreases of 71% and 62% in yield strength compared to that of the neat ABS and ABS80, respectively.

### 3.2.2 | Three-point bending test

In Figure 7, the stress–strain diagrams for neat ABS, ABS80, ABS60, and TPU under three-point bending mode are presented. TPU shows a completely linear behavior and due to the limited amount of strain in the bending loading

mode, the material does not enter the plastic range. According to Figure 7, there is a significant difference in the bending behavior of the three neat ABS and ABS-TPU compounds in the elastic region and the yield stress. However, due to the limited amount of strain and the combination of tensile and bending loading, the comparison of materials in the plastic region is not considered. The slope of the linear region and the yield stress for ABS is the highest value, and this trend decreases with the increase in the amount of TPU in ABS-TPU compounds. Additionally, the behavior of ABS80 tends to be more similar to neat ABS. In general, although adding TPU could moderately increase the strain, it significantly reduces the yield strength.

### 3.3 | Fracture toughness

Figure 8 shows the force–crack growth diagrams for neat ABS and TPU, as well as softened and blended 3D-

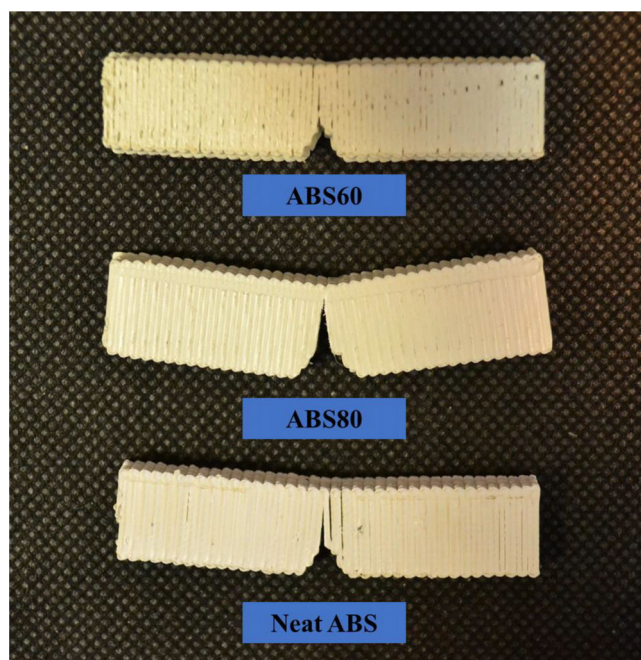


**FIGURE 9** Single-edge notched bending samples after fracture test under three point bending loading mode.

printed ABS with 20 and 40 wt% of TPU. This trend is consistent with the mechanical behavior observed in other loading modes, such as bending, tensile, and compression tests. The sharp decrease in force is also evident in the slope of the linear region (elastic section) of the samples when 20 and 40 wt% TPU are added.

The maximum force for crack growth initiation for neat ABS, TPU, ABS80, and ABS60 is 568.4, 48.5, 335.3, and 123.2 N, respectively. These values indicate the material's resistance against crack growth initiation, which decreases as the amount of TPU increases. Additionally, the force–crack growth diagram can be divided into two parts: the linear or elastic region and the nonlinear region. As mentioned earlier, the linear region of the samples continues until reaching the peak force and then decreases. At this point, the behavior of all three ABS and ABS-TPU compounds becomes completely different. The curve slope is steep for ABS and becomes slight for ABS80 and ABS60. This region represents the material's resistance to crack growth, and therefore, a nonlinear and different behavior is observed in the three compounds. Neat ABS exhibits a completely brittle behavior, whereas ABS60 is completely soft and tough, showing more resistance to crack growth.

In Figure 9, the printed SENB samples after the fracture toughness test show uniform crack growth aligned with the loading direction for all three samples. The stable crack growth in the same direction as the loading direction confirms the accuracy and feasibility of the test

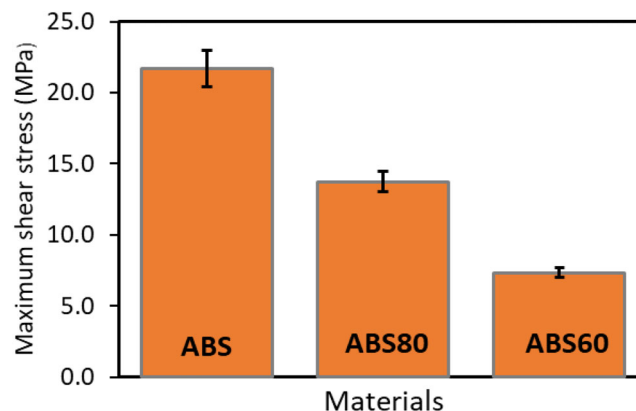


**FIGURE 10** Shear strength of the neat ABS and the ABS-TPU blends.

for calculating the fracture toughness value. According to this figure, it is evident that the crack propagation in ABS60 is less than that of ABS and ABS80, which is in accordance with previous results that showed adding TPU changed the ABS behavior from brittle to ductile.

The fracture toughness value was calculated using Equation (1), where  $K_Q$  is the fracture toughness value,  $P_Q$  is the maximum force,  $B$  is the thickness, and  $W$  is the width of the SENB sample. Additionally,  $f(x)$  is a function of the ratio of the initial crack ( $a$ ) to the sample width ( $W$ ). The fracture toughness values for neat ABS, ABS80, and ABS60 were determined to be 7.92, 4.50, and 1.72 MPa m<sup>1/2</sup>, respectively.

$$K_Q = \left( \frac{P_Q}{BW^{3/2}} \right) f(x). \quad (1)$$

### 3.4 | Shear test and SEM

The strength and adhesion force between the rasters of the 3D-printed samples are key criteria for evaluating the printability and mechanical properties of the materials. To assess the adhesion between the printed layers and, therefore, the printability, a shear test was conducted on 3D-printed neat ABS and toughened ABS with 20 and 40 wt% of TPU. The results are shown in Figure 10.

According to Figure 10, the shear strength of the neat ABS, ABS80, and ABS60 blends is demonstrated with average values of 21.7, 13.7, and 7.3 MPa, respectively, which are acceptable for polymeric materials. Figure 10 also shows that the shear strength decreases with the addition of 20 and 40 wt% of TPU. By adding 40 wt% of TPU, the shear strength of ABS decreases by about 66%.

Figure 11 also shows SEM images of the cross-sections of neat ABS and ABS-TPU blends. These samples exhibit microholes caused by FDM printing and the



viscosity of ABS-TPU compounds, which occur regularly between the overlapping layers. Figure 11 demonstrates that the printing quality and diffusion between printed layers are excellent for all samples. This phenomenon is attributed to the low viscosity of materials during the printing procedure, resulting from the high printing temperature of 240°C.<sup>32,33</sup>

Furthermore, the addition of TPU to the ABS matrix significantly reduces the viscosity of the blends, leading to improved quality of the printed parts and bonding between layers. As is clear from the SEM images, adding TPU to ABS reduces the size and number of voids. It means that TPU addition reduces the occurrence of voids between rasters in the ABS-based blend specimen. Moreover, increasing the TPU content in the blends enhances the diffusion between layers and rasters, resulting in smaller voids.

However, even with the addition of 40 wt% of TPU, there are still some microvoids present in the SEM images. Removing these microholes and voids in the FDM printing process is challenging due to the rapid cooling and shrinkage of the raster after deposition. It has been a persistent challenge for the past two decades. In addition to the FDM printing mechanism, printing parameters and thermoplastic rheology also aggravate this challenge. These factors influence the feeding rate and extrusion process, which in turn affect the formation

of microholes. Furthermore, the nonuniform morphology of ABS-TPU exacerbates rheological changes and the disconnection and connection of feeding conditions in FDM 3D printing. The presence of larger TPU droplets intensifies this challenge.

The morphology images of the ABS80 and ABS60 blends are illustrated in Figure 12. By integrating the results from Figures 11 and 12, it can be deduced that the differences in shear strength among these parts are mainly associated with the stiffness of the materials used. Based on the findings from the uniaxial tensile and compression tests, the neat ABS has the highest strength, whereas the ABS60 blend has the lowest strength among these three materials. The matrix-droplet morphologies and the average diameter of TPU droplets, which is about 1 μm, indicate good compatibility between ABS and polyester-based TPU. This suggests that the TPU affects the mechanical characteristics of the material, resulting in the softening of the blends. Therefore, it is logical that this trend is also observed in shear strength.

Although the area of voids has a minor impact on the shear strength of these materials due to the perfect bonding between layers in all three samples, the shear strength of the neat ABS and the ABS80 blend can be improved by reducing the area of voids, similar to the ABS60 blend, by printing these two specimens at a higher

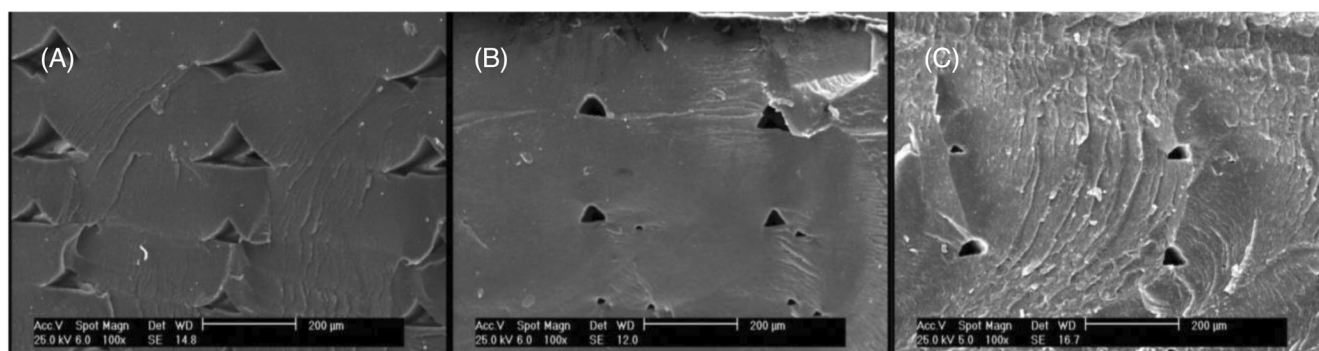


FIGURE 11 Scanning electron microscopy of (A) the neat ABS, (B) the ABS80 blend, and (C) the ABS60 blend.

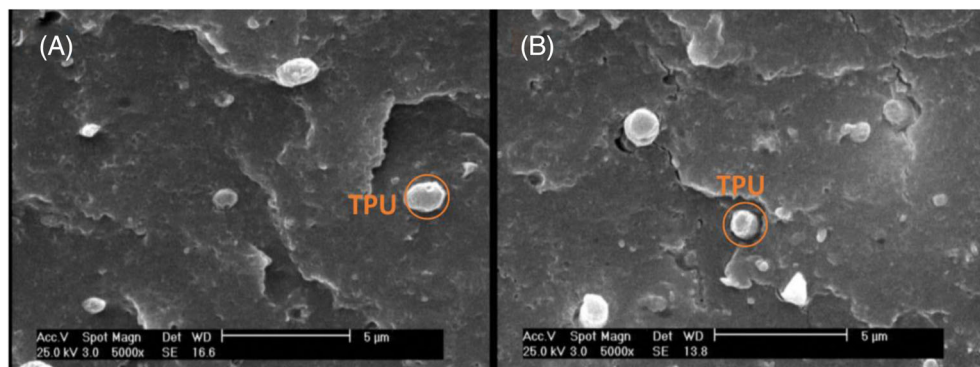


FIGURE 12 Scanning electron microscopy of the morphology of (A) the ABS80 blend and (B) the ABS60 blend.

temperature or increasing the material flow during the printing process.<sup>10,34</sup> However, due to the basic concept of FDM, which involves the extrusion of semiliquid thermoplastic, these diamond-shaped voids cannot be eliminated.

## 4 | CONCLUSIONS

Adding 20 and 40 wt% TPU to ABS reduced the glass transition temperature from 118°C for ABS to 114°C for ABS80 and 106°C for ABS60. The addition of TPU also decreased the intensity of the transition temperature peak. Furthermore, at room temperature, the storage modulus decreased from 900 MPa for ABS to 600 MPa for ABS80 when 20 wt% TPU was added.

The results of tensile, compression, and bending tests showed that the addition of TPU decreased the strength of blends. However, it also increased their elongation prior to failure. This implies that ABS-TPU blends have higher formability than pure ABS.

Regarding the fracture toughness tests, the addition of TPU significantly decreased the maximum force needed for crack initiation. For neat ABS, the required force was 568.4 N, whereas, for ABS80, ABS60, and TPU, it declined to 335.3, 123.2, and 48.5 N, respectively. The results also demonstrated that adding TPU had a positive impact on toughening ABS by enhancing the strength of the ABS-TPU blends against crack propagation.

Both SEM images and shear test results confirmed the printability of blends and the acceptable adhesion between the printed layers. Based on the shear test outcomes, although the addition of TPU caused a reduction in shear strength for ABS80 and ABS60 compared with neat ABS, their shear strength still falls within an acceptable range for polymers. The size and number of voids and microholes decrease as the amount of TPU increases. However, it is inevitable to have some voids and holes due to the inherent characteristics of FDM.

## DATA AVAILABILITY STATEMENT

Data sharing is not applicable to this article as no new data were created or analyzed in this study.

## ORCID

Davood Rahmatabadi  <https://orcid.org/0000-0002-6898-3061>

## REFERENCES

- Jiang Y, Zhou J, Shi H, et al. Preparation of cellulose nanocrystal/oxidized dextran/gelatin (CNC/OD/GEL) hydrogels and fabrication of a CNC/OD/GEL scaffold by 3D printing. *J Mater Sci.* 2020;55:2618-2635. doi:10.1007/S10853-019-04186-0/METRICS
- Liu J, Zhou Y, Lu J, et al. Injectable, tough and adhesive zwitterionic hydrogels for 3D-printed wearable strain sensors. *Chem Eng J.* 2023;475:146340. doi:10.1016/J.CEJ.2023.146340
- Song D, Chen X, Wang M, Wu Z, Xiao X. 3D-printed flexible sensors for food monitoring. *Chem Eng J.* 2023;474:146011. doi:10.1016/J.CEJ.2023.146011
- Liu Y, Tan Q, Lin H, et al. Integrated design and additive manufacturing of lattice-filled multi-cell tubes. *Compos Sci Technol.* 2023;243:110252. doi:10.1016/j.compscitech.2023.110252
- Xia BC, Huang X, Chang L, Zhang R, Liao Z, Cai Z. The arrangement patterns optimization of 3D honeycomb and 3D re-entrant honeycomb structures for energy absorption. *Mater Today Commun.* 2023;35:105996. doi:10.1016/j.mtcomm.2023.105996
- Cheng P, Peng Y, Li S, et al. 3D printed continuous fiber reinforced composite lightweight structures: a review and outlook. *Compos Part B Eng.* 2023;250:110450. doi:10.1016/J.COMPOSITESB.2022.110450
- Soleyman E, Aberoumand M, Soltanmohammadi K, et al. 4D printing of PET-G via FDM including tailormade excess third shape. *Manuf Lett.* 2022;33:1-4. doi:10.1016/j.mfglet.2022.05.002
- Yan Z, Hu Q, Jiang F, Lin S, Li R, Chen S. Mechanism and technology evaluation of a novel alternating-arc-based directed energy deposition method through polarity-switching self-adaptive shunt. *Addit Manuf.* 2023;67:103504. doi:10.1016/J.ADDMA.2023.103504
- Singh A, Wang Y, Zhou Y, et al. Utilization of antimony tailings in fiber-reinforced 3D printed concrete: a sustainable approach for construction materials. *Construct Build Mater.* 2023;408:133689. doi:10.1016/J.CONBUILDMAT.2023.133689
- Rahmatabadi D, Ghasemi I, Baniassadi M, Abrinia K, Baghani M. 4D printing of PLA-TPU blends: effect of PLA concentration, loading mode, and programming temperature on the shape memory effect. *J Mater Sci.* 2023;2023:1-17. doi:10.1007/S10853-023-08460-0
- Aberoumand M, Soltanmohammadi K, Soleyman E, et al. A comprehensive experimental investigation on 4D printing of PET-G under bending. *J Mater Res Technol.* 2022;18:2552-2569. doi:10.1016/J.JMRT.2022.03.121
- Rahmatabadi D, Aberoumand M, Soltanmohammadi K, et al. Toughening PVC with biocompatible PCL softeners for supreme mechanical properties, morphology, shape memory effects, and FFF printability. *Macromol Mater Eng.* 2023;308:2300114. doi:10.1002/MAME.202300114
- Cheng P, Peng Y, Wang K, Le Duigou A, Ahzi S. 3D printing continuous natural fiber reinforced polymer composites: a review. *Polym Adv Technol.* 2024;35:e6242. doi:10.1002/PAT.6242
- Li S, Cheng P, Ahzi S, et al. Advances in hybrid fibers reinforced polymer-based composites prepared by FDM: a review on mechanical properties and prospects. *Compos Commun.* 2023;40:101592. doi:10.1016/J.COCO.2023.101592
- Stiltner LJ, Elliott AM, Williams CB. A Method for Creating Actuated Joints via Fiber Embedding in a Polyjet 3D Printing Process. 2011. doi:10.26153/tsw/15319
- Siqueiros JG, Schnittker K, Roberson DA. ABS-maleated SEBS blend as a 3D printable material. *Virtual Phys Prototyp.* 2016;11:123-131. doi:10.1080/17452759.2016.1175045

17. Torrado Perez AR, Roberson DA, Wicker RB. Fracture surface analysis of 3D-printed tensile specimens of novel ABS-based materials. *J Fail Anal Prev.* 2014;14:343-353. doi:10.1007/s11668-014-9803-9
18. Rocha CR, Torrado Perez AR, Roberson DA, Shemelya CM, Macdonald E, Wicker RB. Novel ABS-based binary and ternary polymer blends for material extrusion 3D printing. *J Mater Res.* 2014;29:1859-1866. doi:10.1557/JMR.2014.158
19. Andrade Chávez F, Siqueiros JG, Carrete IA, Delgado IL, Ritter GW, Roberson DA. Characterisation of phases and deformation temperature for additively manufactured shape memory polymer components fabricated from rubberised acrylonitrile butadiene styrene. *Virtual Phys Prototyp.* 2018;14:188-202. doi:10.1080/17452759.2018.1550694
20. de León AS, Domínguez-Calvo A, Molina SI. Materials with enhanced adhesive properties based on acrylonitrile-butadiene-styrene (ABS)/thermoplastic polyurethane (TPU) blends for fused filament fabrication (FFF). *Mater Des.* 2019;182:108044. doi:10.1016/J.MATDES.2019.108044
21. Thavornytikarn B, Aumnate C, Kosorn W, Nampichai N, Janvikul W. Acrylonitrile butadiene styrene/thermoplastic polyurethane blends for material extrusion three-dimensional printing: effects of blend composition on printability and properties. *ACS Omega.* 2023;8:45013-45025. doi:10.1021/ACSOMEGA.3C06595
22. Weng Z, Wang J, Senthil T, Wu L. Mechanical and thermal properties of ABS/montmorillonite nanocomposites for fused deposition modeling 3D printing. *Mater Des.* 2016;102:276-283. doi:10.1016/J.MATDES.2016.04.045
23. Zhu J, Hu Y, Tang Y, Wang B. Effects of styrene-acrylonitrile contents on the properties of ABS/SAN blends for fused deposition modeling. *J Appl Polym Sci.* 2017;134:134. doi:10.1002/APP.44477
24. Akato K, Tran CD, Chen J, Naskar AK. Poly(ethylene oxide)-assisted macromolecular self-assembly of lignin in ABS matrix for sustainable composite applications. *ACS Sustain Chem Eng.* 2015;3:3070-3076. doi:10.1021/ACSSUSCHEMENG.5B00509/SUPPL\_FILE/SC5B00509\_SI\_001.PDF
25. Yin J, Lu C, Fu J, Huang Y, Zheng Y. Interfacial bonding during multi-material fused deposition modeling (FDM) process due to inter-molecular diffusion. *Mater Des.* 2018;150:104-112. doi:10.1016/J.MATDES.2018.04.029
26. Ratiu M, Prichici MA, Anton DM, Negrau DC. Compression testing of samples printed on Delta and Cartesian 3D printer. *IOP Conference Series: Materials Science and Engineering.* 2021;1169(1):012008. doi:10.1088/1757-899x/1169/1/012008
27. He F, Thakur VK, Khan M. Evolution and new horizons in modeling crack mechanics of 3D printing polymeric structures. *Mater Today Chem.* 2021;20:100393. doi:10.1016/J.MTCHEM.2020.100393
28. Song Y, Li Y, Song W, Yee K, Lee KY, Tagarielli VL. Measurements of the mechanical response of unidirectional 3D-printed PLA. *Mater Des.* 2017;123:154-164. doi:10.1016/J.MATDES.2017.03.051
29. ASTM D5045. Fracture Toughness and Strain Energy Release Rate of Plastic Materials. Accessed July 3, 2022. <https://www.testresources.net/applications/standards/astm/astm-d5045-fracture-toughness-and-strain-energy-release-rate-of-plastic-materials/>
30. Torres J, Cole M, Owji A, DeMastry Z, Gordon AP. An approach for mechanical property optimization of fused deposition modeling with polylactic acid via design of experiments. *Rapid Prototyp J.* 2016;22:387-404. doi:10.1108/RPJ-07-2014-0083
31. Gnatowski A, Gołębski\* R, Sikora P. Analysis of thermomechanical properties of polymeric materials produced by a 3D printing method. *Teh Glas.* 2019;13:343-348. doi:10.31803/TG-20191102120738
32. Harris CG, Jursik NJS, Rochefort WE, Walker TW. Additive manufacturing with soft TPU – adhesion strength in multimaterial flexible joints. *Front Mech Eng.* 2019;5:37. doi:10.3389/FMECH.2019.00037/BIBTEX
33. Rahmatabadi D, Ghasemi I, Baniassadi M, Abrinia K, Baghani M. 3D printing of PLA-TPU with different component ratios: fracture toughness, mechanical properties, and morphology. *J Mater Res Technol.* 2022;21:3970-3981. doi:10.1016/j.jmrt.2022.11.024
34. Rahmatabadi D, Soltanmohammadi K, Pahlavani M, et al. Shape memory performance assessment of FDM 3D printed PLA-TPU composites by Box-Behnken response surface methodology. *Int J Adv Manuf Technol.* 2023;127:935-950. doi:10.1007/s00170-023-11571-2

**How to cite this article:** Soltanmohammadi K, Rahmatabadi D, Aberoumand M, et al. Effects of TPU on the mechanical properties, fracture toughness, morphology, and thermal analysis of 3D-printed ABS-TPU blends by FDM. *J Vinyl Addit Technol.* 2024;1-11. doi:10.1002/vnl.22097